



Stabilization of Stainless Steel Slag via Air Granulation

Mikael Lindvall¹ · Lily Lai Chi So² · Mahdi Mahdi² · Janice Bolen² · Johannes Nell² · Isabelle Nolet² · Darryl Metcalfe² · Sina Mostaghel^{2,3} · Olle Sundqvist⁴

Published online: 8 February 2019
© The Minerals, Metals & Materials Society 2019

Abstract

In stainless steel production, slag from argon oxygen decarburization (AOD) converters is dumped on to the ground and then slowly cooled. The slag undergoes phase transformation from β -dicalcium silicate (β -C₂S) to γ -dicalcium silicate (γ -C₂S) at approximately 500 °C to 450 °C, resulting in slag volume expansion, disintegration, and dust generation. The dusty slag leads to challenges in material handling, metals recovery, and emissions control. Some operations use slag additives to stabilize slag, but this solution is expensive and can limit the end use of slag due to inclusion of toxic elements. Air granulation was hypothesized as a water-free method for stabilizing AOD slag via rapid quenching. Pilot-scale experiments at Sandvik Materials Technology (SMT) with silicon-reduced AOD slags confirmed that air granulation can produce products which are stable and dust free. Mineralogical analyses further indicated that these air-granulated stainless slags contained either no or low content of γ -C₂S and are therefore stable.

Keywords Slag · Stainless · Argon oxygen decarburization · Dry granulation

Introduction

Argon oxygen decarburization (AOD) slag results from the production of stainless steel and is commonly dumped on to the ground and then slowly cooled through natural convection air cooling. AOD slag typically contains dicalcium silicate, Ca₂SiO₄ (C₂S), which is present in difference phases, as shown in Fig. 1. During the slow cooling, C₂S undergoes a polymorphic solid-phase transition from α -C₂S to β -C₂S at approximately 600 °C to 700 °C and then from β -C₂S to γ -C₂S at 450 °C to 500 °C [1–3]. The transformation of β -C₂S to γ -C₂S results in volume increase in the range of 10% to 12% and generates high internal stresses due to difference in the crystal structures and molar volumes

(or density) between phases—this results in disintegration of slag into a dusty powder [2, 3]. The dusty slag leads to operational challenges in material handling and metal recovery, and environmental challenges in controlling emissions.

To address the challenges of dusty AOD slag, some operations use chemical methods to prevent C₂S-driven disintegration based on incorporating doping elements such as borate in the C₂S crystal [4, 5]. Although only up to 0.25 wt% of borate is required for stabilization of AOD slag, the use of this additive represents a significant cost to the operation [6]. Furthermore, boron leaching from slag can have a negative effect on the environment [7]. Non-boron additives to address the challenge of boron leaching, such as P₂O₅, Al₂O₃, Na₂O, K₂O, BaO, MnO₂, and Cr₂O₃, have also been reported [5, 8].

Physical methods, such as rapid quenching of ~5 °C/s, can also be employed to prevent the phase transformation from β -C₂S to γ -C₂S [5, 8, 9]. If AOD slag is rapidly cooled, the crystalline domain sizes are reduced, and β -C₂S is stabilized at low temperature, which means volume expansion and disintegration do not occur. Rapid cooling can be achieved by quenching with water, and it was hypothesized that rapid cooling can also be achieved with air. Water granulation of slag is a common practice in ironmaking and other industries in which slag streams are typically devoid of metal. Air

The contributing editor for this article was Sharif Jahanshahi.

✉ Lily Lai Chi So
Lily.So@hatch.com

- ¹ SWERIM AB, Box 812, 971 25 Luleå, Sweden
- ² Hatch Ltd, 2800 Speakman Drive, Mississauga, ON L5K 2R7, Canada
- ³ Present Address: Aurubis AG, 20539 Hamburg, Germany
- ⁴ AB Sandvik Materials Technology, 811 81 Sandviken, Sweden

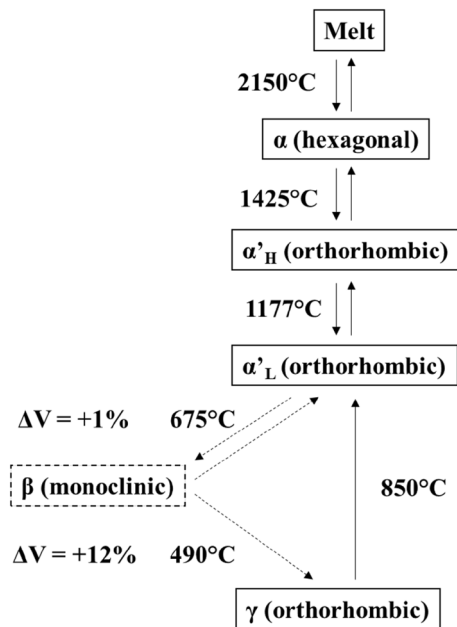


Fig. 1 C_2S -phase transformations during cooling [1]

granulation has been commercialized mostly for electric arc and basic oxygen steelmaking slags, with some penetration into nonferrous markets as well. Since AOD slag typically contains entrained stainless steel metal, water granulation is *not* a safe, viable option, as metal–water contact can result in dangerous steam explosions. Metal entrainment is not a risk with air granulation since it is a dry process, and if rapid cooling can be demonstrably achieved, a viable solution to overcome the problem of dusty AOD slag could be realized.

Air granulation is one of three main dry granulation methods which has been developed over the past few decades [10–15]. Dry granulation methods can be divided into three main areas: (1) mechanical granulation [11, 16], (2) centrifugal granulation [12, 16–21], and (3) air granulation. In mechanical dry granulation, molten slag is broken up and quenched via mechanical means such as rotating drums, blades, or shot materials. An example is the Paul Wurth

mixing method, in which molten slag is mixed with steel spheres, which rapidly cool the slag [11, 16]. In centrifugal dry granulation such as CSIRO's spinning disk and Siemens VAI rotating cup technology, molten slag is ejected radially outwards via centrifugal force, broken up into small droplets, and quenched into solidified granules [16–21]. Although mechanical and centrifugal methods demonstrated promising results at the lab and pilot scales, challenges including scale-up and contact of molten material with mechanical equipment have limited their progress to commercial-scale implementation.

Development of air granulation technology began in the 1970s for steelmaking basic oxygen furnace slag and ferromanganese slag, which proved to be technically and economically viable at the commercial scale [13–15]. Air granulation is a simple process as no mechanical equipment is in contact with molten slag. As shown in Fig. 2, air granulation involves a simple molten slag launder discharging molten slag over an air jet, which breaks up and quenches the molten slag. The slag granules are contained in an enclosure for periodic or continuous collection. The granulation air passes concurrently relative to the slag granules to obtain a hot gas stream of approximately 400 °C, which can be directed to equipment that recovers or uses the heat energy. Currently, air or gas granulation of AOD slag is not implemented at the commercial scale. Small-scale air- and gas-granulation experiments of AOD slag have been carried out in previous studies [14, 22]. These experimental results suggested that rapid cooling is sufficient with gas granulation to limit the transformation of β - C_2S to γ - C_2S thereby resulting in a stable, dust-free, AOD slag product. However, commercial-scale conclusions cannot be drawn from small-scale experiments. Re-melting of slag may have altered slag chemistry, and process parameters tested under smaller-scale conditions may not be reflective of the commercial-scale process, both of which may lead to erroneous results. These challenges can be addressed by larger onsite pilot-scale experimentation using molten slag obtained directly from production without re-melting, and where the scale of testing involved closer reflects that of a commercial-scale operation.

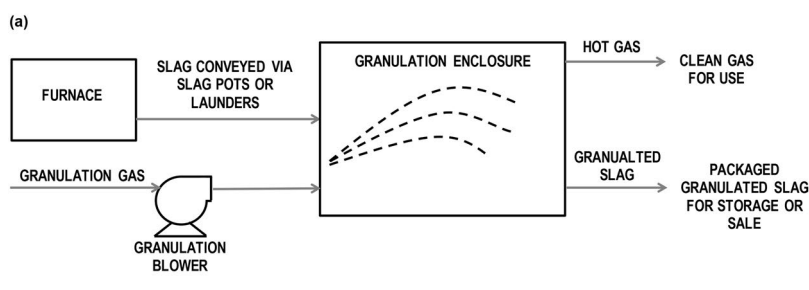


Fig. 2 **a** Schematic of air granulation process. **b** Commercial operation of a Hatch-designed air granulation system (Color figure online)

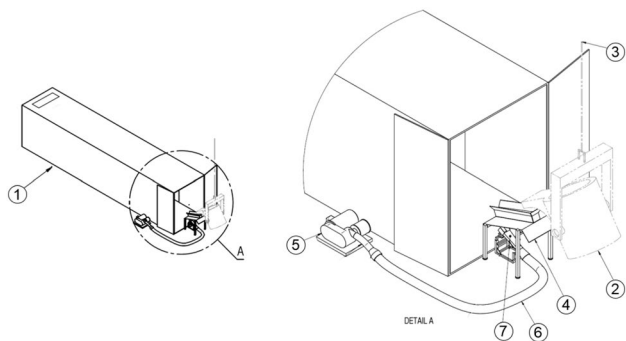


Fig. 3 Schematic of the onsite pilot-scale air granulation system

Experimental

Equipment

The onsite pilot-scale air granulation system designed by Hatch were erected and operated by SWERIM together with Sandvik Materials Technology (SMT) and Harsco at SMT's plant in Sandviken. The system was designed to process at the rates ranging from 15 kg/min to 30 kg/min of AOD slag depending on the specific air-to-slag ratio. The system consisted of the following components, as shown in Fig. 3:

1. a granulation enclosure to collect granulated slag product;
2. a tilting ladle to transport slag;
3. a crane to transport the tilting ladle;
4. a slag feeding launder to receive the slag from the tilting ladle;
5. a blower with variable speed drive to supply granulation air;
6. a flexible hose connecting the blower to the granulation air nozzle; and
7. a granulation air nozzle and support.

The granulation enclosure consisted of a modified 20-foot sea container. The floor and back wall of the container were lined with steel sheet. An off-gas ventilation hood was installed at the rear roof of the container. A manual tilting 0.7 m³ ladle equipped with a spout was used for transporting slag. The ladle wall, bottom, and spout were lined with Al₂O₃-based brick, high alumina gun mix, and high castable alumina. The ladle was lifted with a crane equipped with a crane scale. A blower with variable speed drive supplied air through a flexible hose to an adjustable air nozzle for granulation. A slag feeding launder constructed of steel plate was located above the air nozzle, such that molten slag can be discharged in front of the air stream. In addition, a splash guard in the form of a cone with castable alumina was

constructed for enabling direct and accurate slag tap from the AOD converter to the tilting ladle.

Pilot-Scale Air Granulation Test Procedure

A 2-week test campaign was carried out at SMT using silicon-reduced AOD slags. In the AOD process, by adjusting the O₂/Ar ratio, a small fraction of Cr is reoxidized and moves to slag which is undesirable. To return the Cr back to the alloy and without dissolving too much C in the alloy, metallic reductants such as Si is used. The slag resulting from AOD batches that uses Si is considered as Si-reduced AOD slags.

Si-reduced AOD slags were tapped directly from the production furnace at SMT into the tilting ladle equipped with the splash guard, then transported to the test site for the pilot-scale granulation system, at which point the splash guard was removed with the front-end loader. For the first test of each day, the ladle was preheated by charging hot slag solids into the ladle and placing a lid on the ladle. After several hours of preheat, the hot slag solids were discharged, and the molten AOD slag was tapped from production into the ladle. The ladle was transported to the pilot-scale air granulation system and manually tilted to discharge the molten slag onto the slag feeding launder at rates ranging from 15 kg/min to 30 kg/min, as shown in Fig. 4. The blower speed and the air nozzle dimensions were adjusted to supply the air at particular volumetric flow rates and velocities. The molten slag was granulated by air, and the produced granules were collected in the enclosure. Typical granulation test durations ranged from 5 to 10 min. After the granulation test was completed, the remaining slag in the ladle was



Fig. 4 Photograph of onsite pilot-scale air granulation testing at SMT (Color figure online)

poured out in a nearby pit, and the granules in the enclosure were collected.

Process Parameter Measurements

Slag discharge rate was calculated using the mass of slag discharged from the ladle (as measured at one-minute intervals using a 10-ton crane scale with a resolution of 5 kg) and the granulation duration. An example of slag discharge rate measured during an air granulation test is shown in Fig. 5. Velocity and volumetric flow rate of granulation air were measured using a pitot tube and analog manometer.

Initial attempts to measure molten slag stream temperature were made using high-performance expendable temperature sensors (Heraeus Electro-Nite). However, reliable measurement was not achieved as slag froze quickly on to the sensor tip. An infrared noncontact thermometer (Optris P20) was also tested, but the molten slag stream was too thin to afford any accurate measurement. High-precision thermal camera (Agema Thermovision 550, with emissivity set to 0.95) was ultimately used for molten slag stream and slag granule temperature measurements.

Two K-type thermocouples were installed on the floor of the enclosure (accuracy of ± 1 °C, sampling rate of 5 s), as shown in Fig. 6. Thermocouples, TC1 and TC2, were installed on the floor liner, 570 mm from the side of the enclosure, in the middle, and the rear of the container

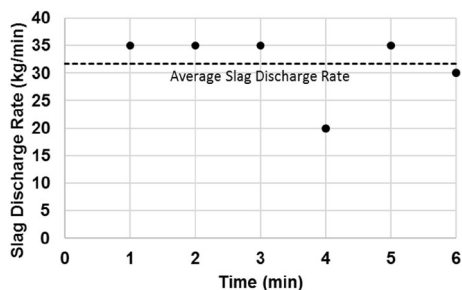
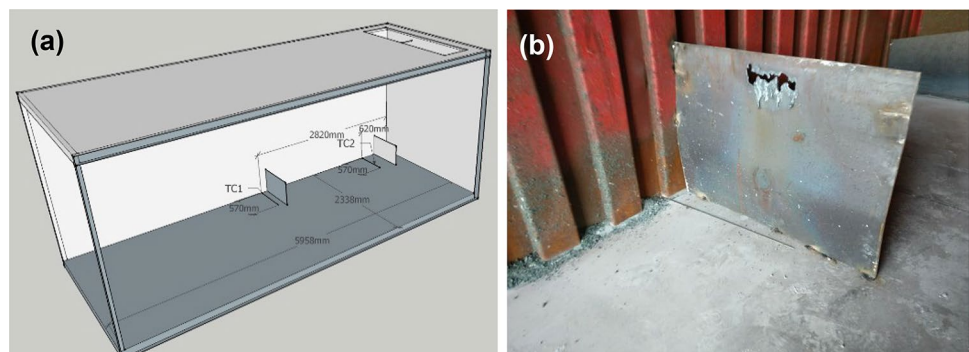


Fig. 5 Example of slag discharge rate during air granulation test. Example shown represents Test 15-A1

Fig. 6 **a** Schematic of granulation enclosure interior with thermocouple locations. **b** Photograph of TC1 and back plate (Color figure online)



to obtain slag granule temperature upon landing. Initial testing showed that TC1 and TC2 were not completely covered with slag granules, and as such, recorded temperatures were influenced by broth slag granule and surrounding air temperature. As such, back plates were installed behind TC1 and TC2 to allow slag granules to be collected at the locations of the thermocouples.

Slag Sampling and Analysis

In all tests, two slag samples were collected—Sample A (granulated slag sample obtained from the granulation enclosure.) and Sample B (reference sample obtained from natural convection air cooling of slag from the ladle). In some tests, an additional sample was collected—Sample W (reference sample obtained from water quenching of slag from the ladle). For several tests, Sample A (granulated slag) was collected as three fractions based on its locational distance from the granulation air nozzle—0 m to 2 m, 2 m to 4 m, and 4 m to 6 m.

Sieve analysis was carried out at SWERIM with sieve sizes of 4000 μm , 2800 μm , 2000 μm , 1400 μm , 1000 μm , 710 μm , 500 μm , and 125 μm . The fraction less than 125 μm was regarded as disintegrated material (dusty slag) and was used as a measure of success of slag stabilization.

Chemical analyses of the collected samples were determined via X-ray fluorescence (XRF) by the SMT plant laboratory.

Mineralogical and phase distribution analyses were carried out via X-ray diffraction (XRD). For phase evaluation, a semi-quantitative approach was used, which is based on the relative peak intensity and their theoretical reference intensity ratios. Samples 14–18 were analyzed at Degerfors Lab and Samples 6–8 were analyzed at the division of Minerals and Metallurgical Engineering at the Lulea University of Technology (LTU).

Results and Discussion

16 tests were completed with Si-reduced slags. Results and observations are summarized in Table 1, and Figs. 7 and 8.

Based on experimental observations, the 16 tests were divided into two categories—slags with apparent low viscosity (12 tests) and slags with apparent high viscosity (4 tests). During the testing of the apparent low-viscosity slags (with low-basicity $\text{CaO}/\text{SiO}_2 = 1.2\text{--}1.7$), slag flow rate could be easily controlled. As such, tests under varying air-to-slag ratio conditions were conducted. However, the apparent high-viscosity slags (with high-basicity $\text{CaO}/\text{SiO}_2 = 1.9\text{--}2.4$) were difficult to pour at controlled flow rates as slag freezing occurred both in the ladle spout and

the launder. As such, only low air-to-slag conditions were tested.

The observed difference in viscosities is consistent with the topology of the liquidus surface in the $\text{CaO}\text{--}\text{MgO}\text{--}\text{SiO}_2$ system, shown in Fig. 9, where liquidus temperature is sensitive to small changes in $\text{CaO}\text{--}\text{MgO}\text{--}\text{SiO}_2$ ratio. As shown in Table 1, slag temperatures during testing were measured for the four low-basicity slag tests (CaO/SiO_2 of 1.6 to 1.7), with temperatures ranging from 1485 °C to 1590 °C. This temperature range is slightly lower than the liquidus temperature for slags in this basicity range (~ 1800 °C). The slag temperatures during testing for high-basicity slags ($\text{CaO}/\text{SiO}_2 > 1.9\text{--}2.0$) are expected to be in a similar range. However, liquidus temperatures for slags with higher basicity are much higher (1900 °C to 2100 °C). Please note that the liquidus temperature is for the ternary $\text{CaO}\text{--}\text{MgO}\text{--}\text{SiO}_2$

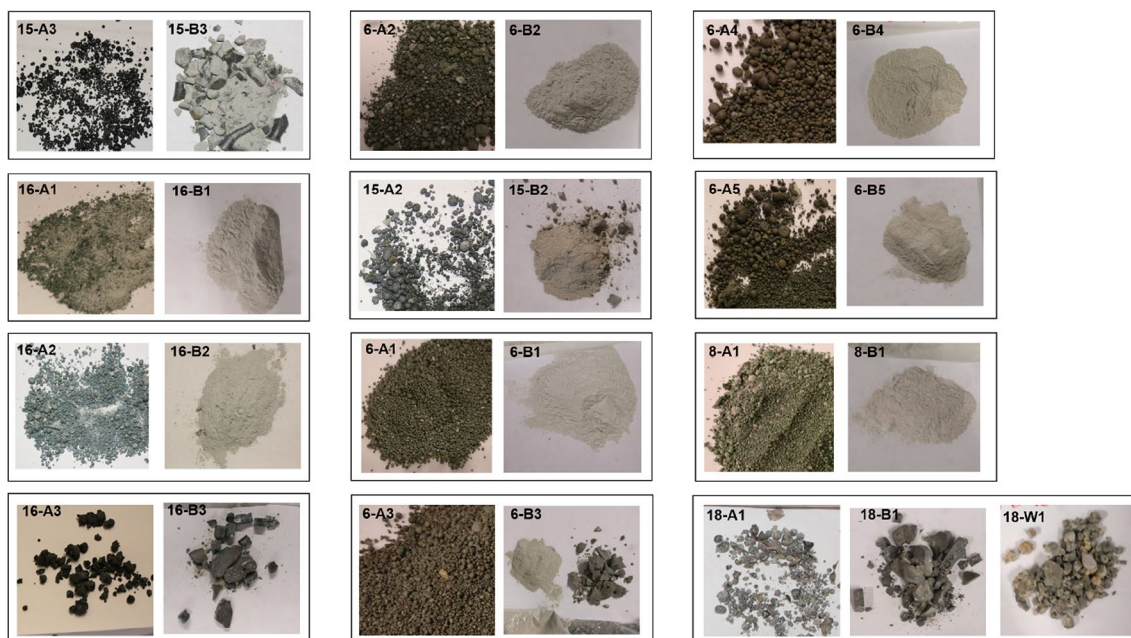
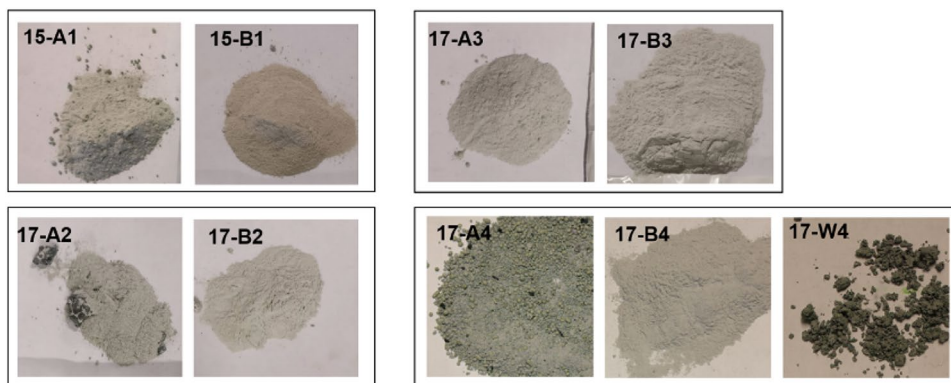


Fig. 7 Low-viscosity slag samples (Color figure online)

Fig. 8 High-viscosity slag samples (Color figure online)



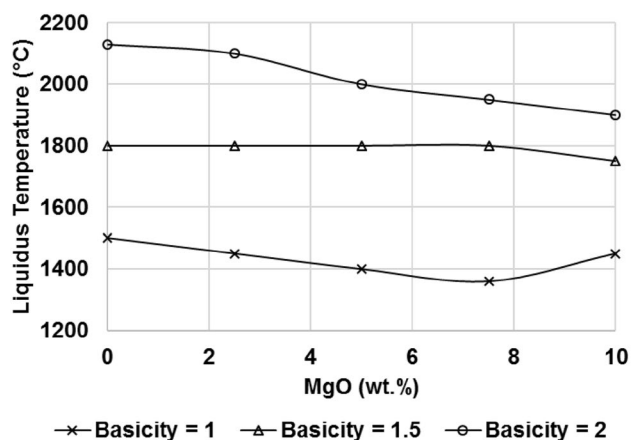


Fig. 9 Liquidus temperatures in the ternary CaO-MgO-SiO₂ system as calculated using FactSage 7.2

system, while the tested system contains other compounds that impact the liquidus, most importantly CaF₂. As such, at the time of testing, the higher-basicity slags were likely at temperatures much lower than their liquidus temperature and with higher solid fractions, leading to an observed higher viscosity.

To support the observed differences in viscosities between low- and high-basicity slags, viscosities for two low-basicity slags (Sample 15-A3 and Sample 6-A5) and two high-basicity slags (Sample 17-A4 and Sample 15-A1) were calculated. First, liquidus temperatures, solid fractions, and viscosities in the estimated tapping temperature range (minimum of 1485 °C to maximum of 1590 °C) and/or at the measured slag tapping temperature were calculated using FactSage 7.2. The model can only predict the viscosities of fully liquid slags. As such, the Einstein–Roscoe equation was used to recalculate the viscosities of liquids containing solid particles, under the assumption of spherical particles of uniform size [23–27]. It must be noted that the calculated viscosities are estimated values due to the inhomogeneity in distribution and the particle sizes in the actual slag melts.

As shown in Table 1, Sample 15-A3 (basicity of 1.3, with low observed viscosity) has an estimated liquidus temperature of 1486 °C and expectedly, no solid fractions in the estimated tapping temperature range of 1485 °C to 1590 °C. The calculated viscosity is the lowest, ranging from 0.8 P to 1.3 P. Sample 6-A5 (basicity of 1.6, with low observed viscosity) has an estimated liquidus temperature of 1743 °C. At the measured slag tapping temperature of 1558 °C, 42% solid fraction and viscosity of 5.7 P were calculated. For higher-basicity Samples 17-A4 (basicity of 1.9, with high observed viscosity) and 15-A1 (basicity of 2.4, with high observed viscosity), a slightly higher range of liquidus temperatures of 1990 °C and 1724 °C, respectively, were calculated. In the estimated tapping temperatures range of

1485 °C to 1590 °C, 7% to 26%, and 40% to 57% solid fractions were expected for Samples 17-A4 and 15-A1, respectively. Consequently, higher viscosity ranges of 0.9 P to 3.2 P and 3.5 P to 30.5 P were calculated for the Samples 17-A4 and 15-A1, respectively. In general, the high-basicity slags demonstrated higher liquidus temperatures, thereby containing higher solid fractions in the estimated tapping temperature ranges. Estimated effective viscosity increases with the increasing solid fraction, which is in agreement with the trend observed in viscosities between low- and high-basicity slags.

Low-Viscosity Slags

For low-viscosity slags, all slow-cooled reference samples (i.e., Sample B) disintegrated except for Samples 16-B3 and 18-B1. The ability for the two Samples 16-B3 and 18-B1 to remain stable under the slow-cooling condition suggests that the faster-cooled granulated Samples 16-A3 and 18-A1 would also be stable, which was demonstrated in testing.

For the air-granulated samples (i.e., Sample A), disintegration was observed for 4 of the 12 tests with low-viscosity slags (Samples 16-A1, 16-A2, 6-A2, and 8-A1). In the basicity range of interest, α -C₂S is the primary phase to form. During granulation tests, if the slag is below its liquidus temperature, C₂S will decrepitate. The corollary to this is that the slag must be sufficiently above its liquidus temperature for granulation to achieve the desired objective of preventing C₂S phase transformations. As shown in Table 1 and Fig. 9, for the 4 tests where the slag temperature was measured, the slags were below their liquidus temperature when the tests were performed, with Samples 6-A2 and 8-A1 recording the lowest slag temperatures and the highest degrees of disintegration.

Of the four tests where air-granulated samples disintegrated, three were from the low air-to-slag ratio tests (Samples 16-A1, 16-A2, 6-A2) and one was from the high air-to-slag ratio tests (Sample 8-A1). These results suggest that low air-to-slag ratio may not achieve rapid cooling, thus resulting in slag disintegration, whereas high air-to-slag ratio may result in faster cooling rate, and consequently result in a stable slag product. Additional testing is required to confirm this observation. Granulated slag landing temperatures for tests producing disintegrated slags were among the highest, reaching a maximum of up to 660 °C. For all the water-quenched tests, the collected Sample W did not show disintegration.

High-Viscosity Slags

For high-viscosity slags, disintegration of reference Sample B was observed for all test. Disintegration of water-quenched Sample W was observed for one test where this sample was

Table 1 Summary of experimental results and observations

Test	Air velocity	Air-to-slag	Composition, wt%										Slag temp., °C	TCI (max), °C	
			CaO	SiO ₂	Al ₂ O ₃	MgO	CaF ₂	MnO	FeO	Cr ₂ O ₃	S	TiO ₂			CaO/SiO ₂
Low-viscosity slags															
15-A3	Low	Low	48	36	2.0	7.6	5.8	0.68	0.5	0.6	5.8	1.3	–	–	286
16-A1	Low	Low	54	32	1.6	8.6	4.0	0.25	<0.5	0.3	0.28	1.7	–	–	–
16-A2	Low	Low	53	31	1.5	8.7	4.1	0.35	<0.5	0.5	0.29	1.7	–	–	–
16-A3	Low	Low	52	31	1.0	9.6	4.0	0.11	<0.5	0.4	0.24	1.7	–	–	–
6-A2	Low	Low	51	31	1.5	8.8	4.3	0.42	0.5	1.0	0.20	1.6	1486	–	661 ^d
15-A2	Low	High	53	32	1.8	10.0	5.8	0.67	<0.5	0.6	0.27	1.7	–	–	144
6-A1	Low	High	49	30	1.1	9.2	5.5	0.36	1.6	1.4	–	0.20	1589	–	383 ^d
6-A3	Low	High	52	30	1.0	9.5	4.6	0.56	<0.5	0.3	0.11	0.37	–	–	302 ^d
6-A4	Low	High	47	30	1.3	9.8	7.9	0.93	<0.5	0.8	–	0.32	–	–	128 ^d
6-A5	Low	High	50	31	1.1	8.2	5.5	0.57	<0.5	0.9	0.15	0.24	1558	–	208 ^d
8-A1	Low	High	51	29	2.0	9.1	4.8	0.49	0.5	1.0	0.29	0.31	1540	–	314 ^d
18-A1	High	Low	42	34	2.7	10	4.2	1.3	0.8	1.8	0.12	1.2	–	–	82
High-viscosity slags															
15-A1	Low	Low	53	22	11.0	7.9	3.9	0.22	<0.5	0.2	0.27	2.4	–	–	451
17-A2	Low	Low	53	27	1.8	11.0	4.2	0.09	1.3	0.4	0.28	2.0	–	–	214
17-A3	Low	Low	53	27	1.3	14.0	4.8	0.07	2.3	0.6	0.22	1.9	–	–	137
17-A4	High	Low	49	26	1.2	13.0	7.0	0.05	1.7	0.5	0.25	1.9	–	–	189

Table 1 (continued)

Test	TC2 (max), °C	d ₈₀ , µm	Colour	Disintegration		Liquidus temp., °C ^b	Solid fraction, % ^b		Viscosity, poise ^c	
				Sample A ^a	Sample B		Sample W	At 1485 °C	At 1590 °C	At 1485 °C
Low-viscosity slags										
15-A3	443 ^d	2700	Black	0.1	Partly	1486	0	0	1.3	0.8
16-A1	–	1500	Green	62	Yes	–	–	–	–	–
16-A2	–	1900	Dark Green	28	Yes	–	–	–	–	–
16-A3	–	> 4000	Black	0	No	–	–	–	–	–
6-A2	546 ^d	2600	Green	34	Yes	–	–	–	–	–
15-A2	315 ^d	2200	Black	1.3	Yes	–	–	–	–	–
6-A1	213 ^d	1800	Green	15	Yes	–	–	–	–	–
6-A3	232 ^d	2100	Black	0	Yes	–	–	–	–	–
6-A4	323 ^d	1400	Black	1.1	Yes	–	–	–	–	–
6-A5	294 ^d	2200	Black	2.1	Yes	1743	–	–	–	5.7
8-A1	230 ^d	1700	Green	28	Yes	–	–	–	–	–
18-A1	410 ^d	> 4000	Black	3.5	No	–	–	–	–	–
High-viscosity slags										
15-A1	820 ^d	Powder	Green	100	Yes	1724	26	7	3.2	0.9
17-A2	500 ^d	Powder	Green	100	Yes	–	–	–	–	–
17-A3	614 ^d	Powder	Green	100	Yes	–	–	–	–	–
17-A4	580 ^d	1050	Green	55	Yes	1990	57	40	30.5	3.5

Bold indicates samples that exhibited disintegration

^awt% fines smaller than 125 µm

^bSolid fraction of slag as calculated using FactSage 7.2. Values calculated at the estimated tapping temperature range (minimum of 1485 °C to maximum of 1590 °C) and/or at the measured slag tapping temperature

^cViscosity of slag as calculated using FactSage 7.2. Values calculated at the estimated tapping temperature range (minimum of 1485 °C to maximum of 1590 °C) and/or at the measured slag tapping temperature

^dBack plate present for TC measurement

Table 2 Particle size distributions of granulated slags

Test	Cumulative passing %								d ₈₀ μm	Disintegration
	125 μm	500 μm	710 μm	1000 μm	1400 μm	2000 μm	2800 μm	4000 μm		
Low-viscosity slags										
15-A3	0.1	2.0	7.6	19.3	38.8	65.6	81.4	90.2	2700	No
16-A1	30.9	41.8	51.0	63.1	77.5	93.3	96	97.3	1500	Yes
16-A2	13.8	24.2	32.3	45.2	60.9	83.2	96.3	99.7	1900	Yes
16-A3	0.0	4.2	10.6	20.0	32.6	48.5	61.2	73.7	> 4000	No
6-A2	17.1	27.2	33.3	42.6	53.7	68.3	82.7	95.7	2600	Yes
15-A2	0.6	11.3	23.4	40.3	57.9	76.6	87.5	95.0	2200	No
6-A1	7.4	15.5	24.1	39.9	61.9	86.1	98.3	99.7	1800	No
6-A3	0.0	7.5	19.3	35.0	55.6	77.9	90.7	98.0	2100	No
6-A4	0.5	17.1	33.8	61.5	79.7	92.2	97.6	99.7	1400	No
6-A5	1.0	13.9	26.5	45.1	61.3	76.5	87.9	95.3	2200	No
8-A1	13.8	28.9	42.1	57.4	73.2	89.5	93.7	95.9	1700	Yes
18-A1	1.7	5.4	7.8	11.2	16.7	27.7	44.8	67.2	> 4000	No
High-viscosity slags										
15-A1	-	-	-	-	-	-	-	-	Powder	Yes
17-A2	-	-	-	-	-	-	-	-	Powder	Yes
17-A3	-	-	-	-	-	-	-	-	Powder	Yes
17-A4	27.4	49.8	62.4	78.5	93.1	98.6	99.5	99.8	1050	Yes

Bold indicate samples that exhibited disintegration

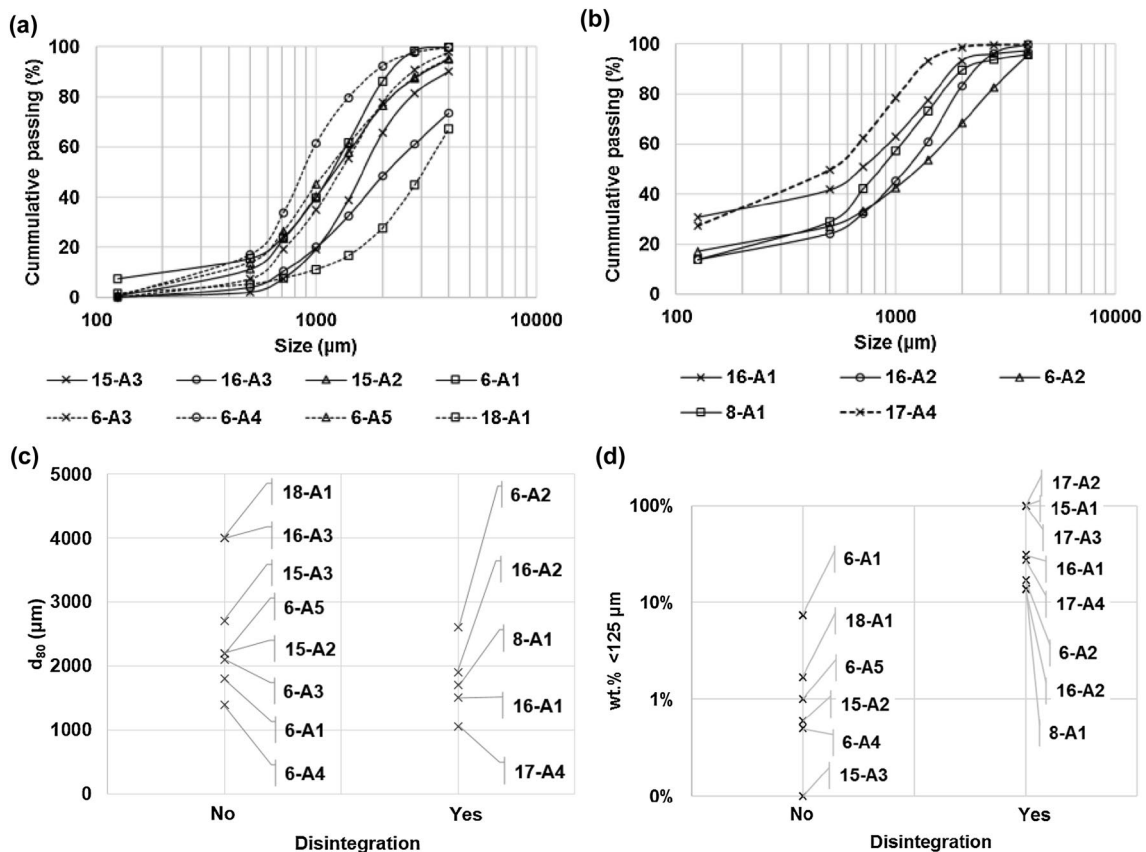


Fig. 10 Particle size distributions for **a** stabilized granulated slags and **b** disintegrated granulated slags. **c** d₈₀ values for granulated slags. **d** wt% of granulated slag less than 125 μm

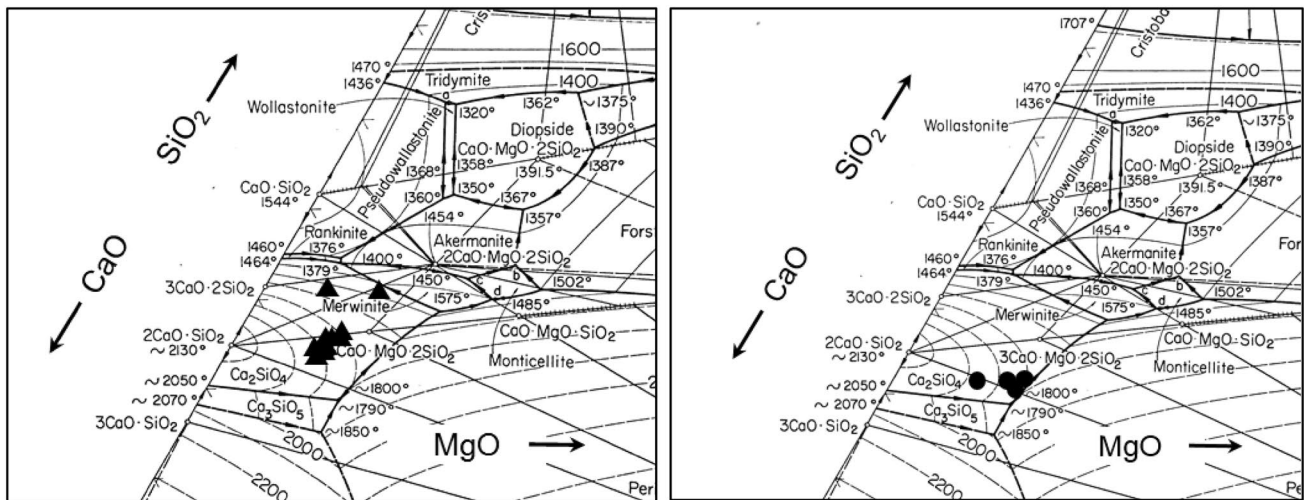


Fig. 11 The normalized low-viscosity slag compositions marked by filled triangle and high-viscosity slag compositions marked by filled circle in the ternary system CaO-MgO-SiO₂ [31]

collected. Similar to low-viscosity slags, this is expected as α -C₂S is the primary phase to form in slags with this basicity range. The entire granulated Sample A disintegrated. Sample 17-A4, which was produced with high air velocity, exhibited improved stabilization. This observation is likely attributed to the ability of higher air velocity to break the slag stream into smaller particles, and the smaller particles being easier to quench. Therefore, higher air velocity improves stabilization of the samples. It must be noted that only one high air velocity test was conducted for low- and high-viscosity slags. Further testing is required to confirm this observation.

Granulated slag landing temperatures were recorded in all the four tests, with the maximum granulated slag landing temperature ranging from 140 to 820 °C. The range of temperatures recorded is attributed to the extent of slag coverage on the thermocouples. TC1 and TC2 were not completely covered with slag granules in initial testing and as such, back plates were installed to allow the slag granules to cover the thermocouples. Lower temperatures in the range of 140 °C to 450 °C were measured by TC1 without a back plate, which may not be representative of true slag landing temperature. Higher temperatures of 500 °C to 820 °C were measured by TC2 with a back plate, which represents true slag landing temperature.

Particle Size Distribution

Particle size distributions (PSD) for granulated slags are shown in Table 2 and Fig. 10. For the tests that generated stabilized slags shown in Fig. 10a, less than 10% of fine particles (< 125 μm) were generated. As shown in Fig. 10c, d₈₀ (80% passing) values for stabilized slags ranged from 2000

to > 4000 μm. The PSD shapes were consistent between tests. For the tests that generated disintegrated slags shown in Fig. 10b, higher fines were generated, with 15–30% of fine particles (< 125 μm) being present. As such, disintegrated slags generally had lower d₈₀ values compared to stabilized slags, as shown in Fig. 10c, and a higher wt% of fine particles (< 125 μm), as shown in Fig. 10d.

Mineralogy

As shown in Table 1, XRF analysis demonstrated that the slags were primarily composed of Si, Ca, and Mg. The ternary system CaO-MgO-SiO₂ was selected to estimate the expected mineral phases in the solidified slag, as shown in Fig. 11. The concentrations of the three components are normalized in proportion to their original fractions with their sum being 100 wt%. As shown in the phase diagram, the slags are in the primary field of C₂S. The presence of C₂S, merwinite (C₃MS₂), C₃S, and periclase (MgO) are expected under equilibrium cooling conditions.

Phase compositions were verified by XRD, as shown in Table 3. Selected granulated Sample A, reference Sample B, and water-quenched Sample W were analyzed. For Samples A and B that demonstrated disintegration, one – 180 μm sample that consisted of disintegrated material and one + 180 μm sample that consisted of stabilized material were analyzed to determine if mineralogy differs between disintegrated and stabilized fractions. Further, for Test 6-A1, two size fractions of stabilized slag, + 180 to 1000 μm and +1000 μm, were analyzed to investigate if mineralogy differs as a function of particle size.

Table 3 Phase composition (by %, or by presence indicated by “x”) of slags determined by XRD

Phase	C ₇ MS ₄	AB ₂ O ₄	C ₃ MS ₂	CaF ₂	γ-C ₂ S	MgO	β-C ₂ S	Ca ₄ Si ₂ F ₂ O ₇	Amorphous	Disintegration	Colour
Low-viscosity slags											
15-A2	7.8		53.2	5.4	12.1	8.9	9.1	Yes	4.0	No	Black
15-B2			62.2	10.8	17.4	5.0			5.0	Yes	Black
15-A3	13.4		46.8	3.2	5.8	4.2	26.4			No	Black
15-B3 ^a			44.2	5.1	6.0					Partly	
16-A1 (- 180 μm)	67.3			5.3	20.8	6.6			19.0	Yes	Green
16-A1 (+ 180 μm)	65.8			7.1		3.9				No	Green
16-B1	31.1			28.1	35.9	4.8		11.3		Yes	Green
16-A2 (- 180 μm)			42.7	9.5	34.2	5.3	6.0		2.0	Yes	Dark Green
16-A2 (+ 180 μm)	41.7		39.9	6.9		4.9	6.6			No	Dark Green
16-B2			50.0	21.2	22.8	6.0				Yes	Dark Green
16-A3 ^b	27.5		8.7				6.3		26.0	No	Black
6-A1 (4–6 m) (- 180 μm)			x	x	x	x				Yes	Green
6-A1 (4–6 m) (180–1000 μm)			x	x		x	x			No	Green
6-A1 (4–6 m) (+ 1000 μm)			x	x		x	x			No	Green
6-B1			x	x	x	x		x		Yes	Green
6-A2 (4–6 m) (+ 180 μm)			x	x	x	x	x		x	No	Green
6-B2			x	x	x	x		x		Yes	Green
6-A3 (4–6 m)		x	x			x				No	Black
6-B3 (- 180 μm)			x	x	x	x				Yes	Black
6-A4 (4–6 m)		x	x			x				No	Black
6-B4			x	x	x	x		x		Yes	Black
6-A5 (4–6 m)		x	x			x				No	Black
6-B5			x		x	x		x		Yes	Black
8-A1 (4–6m) (+ 180 μm)			x	x		x	x		x	No	Green
8-B1			x		x	x		x		Yes	Green
High-viscosity slags											
15-A1	62.0			3.2	22.0	7.3	5.6			Yes	Green
17-A3	18.1			3.8	38.0	32.8	7.3			Yes	Green
17-A4 (- 180 μm)	9.9			5.3	33.3	34.0	17.5			Yes	Green
17-A4 (+ 180 μm)	22.4			8.6	1.0	21.9	38.5		8.0	No	Green
17-B4 ^c	4.7			6.4	34.6	36.8	7.6			Yes	Green
17-W4	31.3			12.6	20.5	14.4	21.2			Partly	

Bold indicate samples that exhibited disintegration

^a44.8% others: 15.0% SiO₂, 5% fluorphlogopite and 29.8% anorthite

^b31.7% others: 2.3% knorringite, 11.2% hatrurite, 11.4% SiO₂ and 6.8% akermanite

^c10% pyrope (M₃A₂S₃)

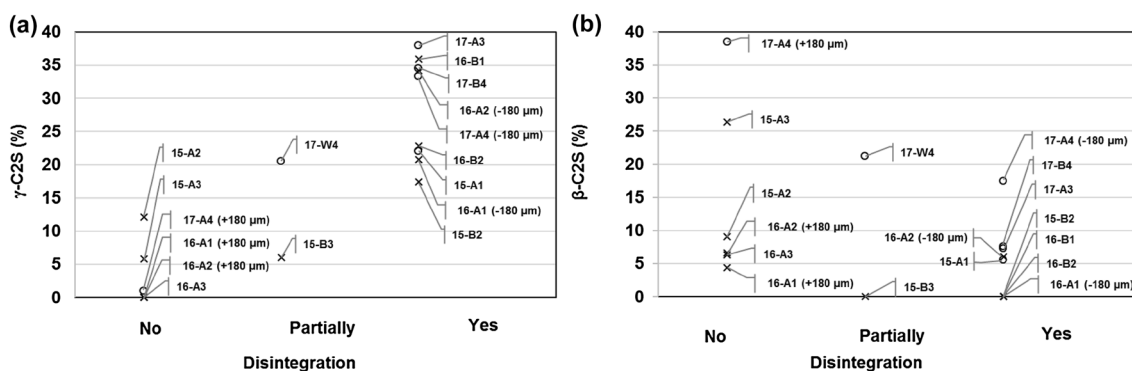


Fig. 12 Comparison of **a** degree of disintegration versus γ -C₂S concentrations and **b** degree of disintegration versus β -C₂S concentrations in slags. Low-viscosity slags are marked by cross symbol and high-viscosity slags are marked by open circle

Table 4 TC1, TC2, and thermal camera-measured slag granule landing temperatures

Test	TC1 °C	TC2 °C	High-precision thermal camera °C	Disintegration	
				wt% of <125 μm	–
Low-viscosity slags					
15-A3	No back plate	443	Not measured	0.1	No
16-A1	No back plate	Not measured	Not measured	62	Yes
16-A2	No back plate	Not measured	Not measured	28	Yes
16-A3	No back plate	Not measured	Not measured	0	No
6-A2	661	546	569	34	Yes
15-A2	No back plate	315	Not measured	1.3	No
6-A1	383	213	391	15	No
6-A3	302	232	< 460	0	No
6-A4	128	323	< 460	1.1	No
6-A5	208	294	< 460	2.1	No
8-A1	314	230	< 460	28	Yes
18-A1	No back plate	410	Not measured	3.5	No
High-viscosity slags					
15-A1	No back plate	820	Not measured	100	Yes
17-A2	No back plate	500	Not measured	100	Yes
17-A3	No back plate	614	Not measured	100	Yes
17-A4	No back plate	580	Not measured	55	Yes

Bold indicate samples that exhibited disintegration

XRD analysis showed that the dominant phases in the slags included C₂S, merwinite (C₃MS₂), bredigite (C₇MS₄), and periclase (MgO), with the balance being CaF₂ and/or cuspidine (Ca₄Si₂F₂O₇). Spinel (AB₂O₄) was present in three low-viscosity slags.

A comparison of degree of disintegration versus γ -C₂S and β -C₂S concentrations is provided in Fig. 12. The stabilized samples had low or no γ -C₂S concentrations (shown in Fig. 12a), with β -C₂S being the dominant C₂S phase (shown in Fig. 12b), indicating limited or no transformation of β -C₂S to γ -C₂S in favor for bredigite and merwinite. Earlier work

has shown that it is possible to prevent disintegration by increasing the MgO content of the slag and thus promoting the formations of both bredigite and merwinite as neither of these minerals disintegrates during cooling in contrast to C₂S [22]. However, the MgO contents in these samples were on a moderate level, and the fact that reference slag formed γ -C₂S shows that the cooling rate has a big impact on the slag mineralogy.

For the stabilized samples with the presence of γ -C₂S (Samples 15-A2, 15-A3, and 17-A4 (+ 180 μm)), stabilization may also be attributed to the presence of bredigite

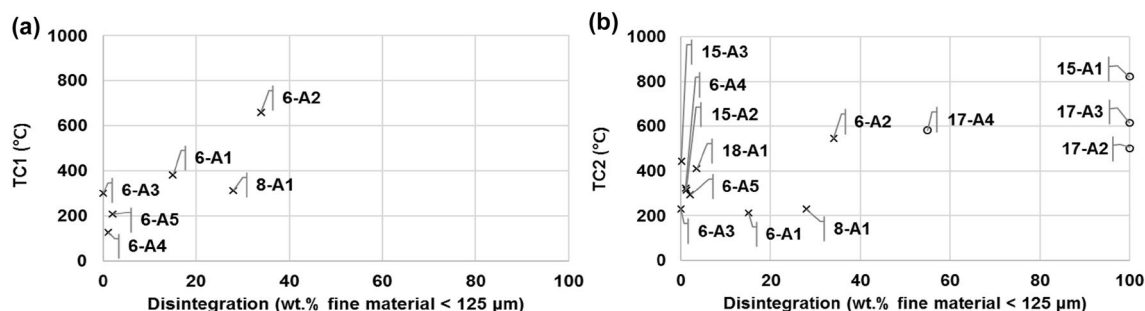


Fig. 13 Comparison of degrees of disintegration versus slag granule landing temperatures measured by **a** TC1 and **b** TC2 for slags. Low-viscosity slags are marked by cross symbol, and high-viscosity slags are marked by open circle

and merwinite [28]. For the reference Sample B, the water-quenched Sample W, and the $-180\ \mu\text{m}$ fractions that demonstrated disintegration, $\gamma\text{-C}_2\text{S}$ was the dominant C_2S phase. As evidenced in Table 3, neither free lime (CaO) nor tricalcium silicate, Ca_3SiO_5 (C_3S), were detected, indicating that disintegration was not the result of hydration of free lime or transformation of C_3S to C_2S . Free MgO was detected in most samples. However, hydration of MgO is a slow process and was unlikely to contribute to the instant disintegration of the Sample B, the Sample W, and the $-180\ \mu\text{m}$ fractions.

The correlation between disintegration and the presence of $\gamma\text{-C}_2\text{S}$ is further evident in the comparison of reference Samples 6-B3, 6-B4, and 6-B5 with their respective granulated Samples 6-A3, 6-A4, and 6-A5, where $\gamma\text{-C}_2\text{S}$ was present in the disintegrated reference samples, but no C_2S was detected in the stable, granulated samples. The comparison of $+180$ to $1000\ \mu\text{m}$ and $+1000\ \mu\text{m}$ size fractions of the Sample 6-A1 showed the same mineralogy for dust-free slag (excluding the $-180\ \mu\text{m}$ fraction), indicating either no or limited influence of particle size on mineralogy on dust-free slag.

Note that the color of the granulated samples may be an indicator of glassiness. Black color indicates more glassiness and hence less decrepitation, which was observed for the stable, granulated low-viscosity slags. Green color indicates more crystallinity and therefore more decrepitation, which was observed for the disintegrated and granulated low-viscosity and high-viscosity slags. The green color may be caused by low levels of Cr^{3+} in the crystal structure of the C_2S [29, 30].

Slag Temperature

Thermocouples, TC1, TC2, and high-precision thermal camera measurements are summarized in Table 4. Thermocouple measurements collected in the presence of back plates enabled slag granules to cover the thermocouples and will be discussed as they better represent the slag

granule temperature. Slag granule landing temperatures were also verified using measurements from a high-precision thermal camera in several tests.

Measurements recorded by the thermocouples were in agreement with those recorded by the thermal camera. Figure 13 shows a comparison of degrees of disintegration, measured in wt% of fine material ($< 125\ \mu\text{m}$), versus slag landing temperature measured by TC1 (in Fig. 13a) and TC2 (in Fig. 13b). Higher slag landing temperature was associated with higher degree of slag disintegration. Slags that landed at temperatures greater than $500\ ^\circ\text{C}$ (Samples 6-A2, 15-A1, 17-A2, 17-A34, and 17-A4) exhibited more than 30 wt% disintegration. Slag that landed at temperatures of greater than $500\ ^\circ\text{C}$ underwent slower cooling and solid-phase transition from $\beta\text{-C}_2\text{S}$ to $\gamma\text{-C}_2\text{S}$ at $450\ ^\circ\text{C}$ to $500\ ^\circ\text{C}$, resulting in disintegration. In contrast, slags that landed at temperatures below $450\ ^\circ\text{C}$ (Samples 15-A3, 15-A2, 6-A1, 6-A3, 6-A4, 6-A5, 8-A1, and 18-A1) exhibited either no or low degree of disintegration. Rapid cooling of the slag to below $450\ ^\circ\text{C}$ seems to have prevented the solid-phase transition from $\beta\text{-C}_2\text{S}$ to $\gamma\text{-C}_2\text{S}$ at $450\ ^\circ\text{C}$ to $500\ ^\circ\text{C}$.

Conclusions

Pilot-scale air granulation testing was completed at Sandvik Materials Technology to determine if fast cooling can be achieved in the air granulation process to prevent the transformation of $\beta\text{-C}_2\text{S}$ to $\gamma\text{-C}_2\text{S}$ and produce stable AOD slag. The pilot-scale air granulation system was able to treat from $15\ \text{kg}/\text{min}$ to $30\ \text{kg}/\text{min}$ of molten slag obtained directly from production.

16 tests were carried out with Si-reduced AOD slags. The main phases in Si-reduced slags include dicalcium silicate (C_2S), CaF_2 , periclase (MgO), merwinite (C_3MS_2), and/or bredigite (C_7MS_4). Mineralogical analyses showed that slow-cooled reference samples underwent solid-phase transition from $\beta\text{-C}_2\text{S}$ to $\gamma\text{-C}_2\text{S}$, resulting in disintegration. Air granulation produced stable slags in several tests,

specifically in those with fast cooling rate conditions of high air-to-slag ratios or high air velocities. The stable granulated slags were rapidly cooled to a landing temperature of less than 450 °C. The granulated slags comprised either no or low γ -C₂S phase or primarily β -C₂S, even though their respective slow-cooled reference samples comprised γ -C₂S. This observation indicated that fast cooling from air granulation prevented the transformation of β -C₂S to γ -C₂S and produced the stable AOD slag. The main Ca–Si-bearing phases in slags with either no or low content of C₂S were those of merwinite and bredigite both of which are not disintegrating. In air granulation tests where disintegrated slags were produced, slag landing temperatures of greater than 500 °C were observed, and high γ -C₂S contents were detected, suggesting that the transformation from β -C₂S to γ -C₂S occurred at temperatures ranging from 450 °C to 500 °C. Neither free CaO nor C₃S was detected, indicating that the disintegration was not the result of free lime hydration or disintegration of C₃S into C₂S. Disintegrated granulated slags were produced primarily during the testing of high-viscosity slags with high basicity. Due to high viscosities, controlled pouring of slag could not be attained, and only the slow cooling rate conditions of low air-to slag ratio could be tested.

The pilot-scale testing results demonstrated that the air granulation process was able to rapidly cool AOD slag to produce a stable dust-free product. Future work will include additional testing and verification for high-viscosity Si-reduced slag using a larger scale system (for slag flow rates of >100 kg/min). It is believed that higher slag pour rates can reduce slag freezing and enable improved control over slag flow rate to test varying slag-to-air ratios. Future work will also include verifying metal recoveries from granulated slag. In the design of industrial air granulation system, process conditions must be optimized such that rapid cooling of slag below 450 °C can be achieved also for high-viscosity slags, thereby preventing transformation from β -C₂S to γ -C₂S and preventing disintegration.

Acknowledgement The authors would like to thank Magnus Eriksson of Harsco and Lennart Johansson of SMT for their support during the execution of the trials. Fredrik Engström of LTU is gratefully acknowledged for support with XRD analysis.

Conflict of interest The authors Lily Lai Chi So, Mahdi Mahdi, Janice Bolen, Johannes Nell, Isabelle Nolet, and Darryl Metcalfe, declare that there are also no conflicts of interest. The authors disclose their employment with Hatch Ltd., a worldwide leading consulting company which provides a wide range of technology-agnostic studies and engineering services, as demonstrated in their execution of a front-end-loaded engineering approach that often involves scaled testing and various studies to first establish project feasibility, taking into consideration various technology solutions, before making recommendations for full-scale implementation. Air granulation, the subject matter discussed in this paper, is one of various technology solutions being studied and recommended by Hatch Ltd. for slag-handling practices.

References

- Chan CJ, Young JF (1992) Physical stabilization of the beta to gamma transformation in dicalcium silicate. *J Am Ceram Soc.* <https://doi.org/10.1111/j.1151-2916.1992.tb04234.x>
- Kim YJ, Nettleship I, Kriven WM (1992) Phase transformations in dicalcium silicate: II, TEM studies of crystallography, microstructure, and mechanisms. *J Am Ceram Soc.* <https://doi.org/10.1111/j.1151-2916.1992.tb05593.x>
- Serjun VZ, Mirtic B, Mladenovic A (2013) Evaluation of Ladle slag as a potential material for building and civil engineering. *Mater Technol* 47(5):543–550
- Huang S, Guo M, Jones PT, and Blanpain B (2013) Fayalite slag modified stainless steel AOD slag. In: *Proceedings of the Third International Slag Valorisation Symposium*, pp. 107–110.
- Pontikes Y, Geysen D (2010) Options to prevent dicalcium silicate-driven disintegration of stainless steel slags. *Arch Metall Mater.* <https://doi.org/10.2478/v10172-010-0020-6>
- Durinck D, Arnout S, Jones PT, Blanpain B, and Wollants P (2008) Borate stabilization of air-cooled slags. *GlobalSlag.* <https://www.globalslag.com/magazine/articles/456-borate-stabilisation-of-air-cooled-slags>. Accessed 24 July 2018.
- Pontikes Y, Kriskova L, Wang X, Geysen D, Arnout S, Nagels E, Cizer, O, Van Gerven T, Elsen J, Guo M, Jones, P.T., and Blanpain B (2011) Additions of industrial residues for hot stage engineering of stainless steel slags. In: *Proceedings of the Second International Slag Valorisation Symposium*, pp. 313–326.
- Engstrom F, Pontikes Y, Geysen D, Jones PT, Bjorkman B, and Blanpain B (2011) Review: Hot stage engineering to improve slag valorisation options. *Proceedings of the Second International Slag Valorisation Symposium*, pp 231–251.
- Kriskova L, Pontikes Y, Pandelaers L, Cizer O, Jones PT, Van Balen K, Blanpain B (2013) Effect of high cooling rates on the mineralogy and hydraulic properties of stainless steel slags. *Metal Mater Trans B.* <https://doi.org/10.1007/s11663-013-9894-9>
- Barati M, Esfahani S, Utigard TA (2011) Energy recovery from high temperature slags. *Energy.* <https://doi.org/10.1016/j.energy.2011.07.007>
- Gajda K, Baunea M, Thöminga J (2017) Recycling options for steel working slag and upcycling perspectives. *Procedia Manuf* 8:643–648
- Lindvall M, Nordberg LO, Stenberg A, Orrling D (2015) SWEREA MEFOS experiences on dry blast furnace slag granulation. In: *Proceedings of the 4th International Slag Valorisation Symposium*, pp 57–61.
- Ando J, Nakahara T, Onoue H, Ichimura S, and Kondo M (1985) Development of slag blast granulation plant characterized by innovation of the slag treatment method, heat recovery, and recovery of slag as resources. *Mitsubishi Heavy Industries, Ltd. Technical Review*, pp 136–142
- Bolen J, Mostaghel S, So L, and Faucher S (2017) Technical and environmental benefits for dry atomization of stainless steel and ladle metallurgy slags. In: *Proceedings for the 2017 Iron & Steel Technology Conference and Exposition*, pp 149–156.
- Hannemann F, Bradfield M, Mahdi M, So L, Metcalfe D (2018) Impact of air granulation on the ferrochrome value chain in metallurgical smelter complexes. *J S Afr Inst Min Metall.* <https://doi.org/10.17159/2411-9717/2018/v118n6a10>
- Kappes H and Michels D (2015) Dry slag granulation and energy recovery. In: *Proceedings of the Fourth International Slag Valorisation Symposium*, pp 39–52.
- Jahanshahi S and Xie D (2012) Current status and future direction of CSIRO's dry slag granulation process with waste heat recovery.

- In: Proceedings for the 5th International Congress on the Science and Technology of Steelmaking 2012 (ICS 2012); CD ROM.
18. Xie D, Pan Y, Flann R, Washington B, Sanetsis S, and Donnelly J (2007) Heat recovery from slag from dry granulation. First Centre for Sustainable Resource Processing Annual Conference, pp 29–30.
 19. Yu PF, Wang SZ (2017) Industrialization mode for energy recovery using dry centrifugal granulation process. *Key Eng Mater* 719:104–108
 20. McDonald IJ and Werner A (2015) Dry granulation with heat recovery. In: Proceedings of the 45th Ironmaking & Mineral Technology Seminar, pp 286–295.
 21. Fleischander A, Fenzl T, and Neuhold R (2018) Dry slag granulation—the future way to granulate blast furnace slag. In: Proceedings of the 2018 Iron & Steel Technology Conference and Exposition, pp 87–94.
 22. Björkman B, Engström F, Larsson M, Yang Q, Ye G, Lindvall M, Hasse B, Roininen J (2012) Stabilization and reuse of AOD-, EAF-, and ladle slag (88033), The Steel Eco-Cycle Scientific Final Report, pp 173–182. https://www.jernkontoret.se/globalassets/publicerat/forskning/d-rapporter/d-853_webb.pdf. Accessed 25 Sept 2018.
 23. Mostaghel S, Matsushita T, Samuelsson C, Bjorkman B, Seetharaman S (2013) Influence of alumina on physical properties of an industrial zinc-copper smelting slag. Part 1—viscosity. *Mineral processing and extractive metallurgy (transactions of the mining and metallurgy: section C)*. <https://doi.org/10.1179/1743285512Y.0000000029>
 24. Mostaghel S, Matsushita T, Samuelsson C, Bjorkman B, Seetharaman S (2013) Influence of alumina on physical properties of an industrial zinc-copper smelting slag. Part 2—apparent density, surface tension and effective thermal diffusivity. *Mineral processing and extractive metallurgy (transactions of the mining and metallurgy: section C)*. <https://doi.org/10.1179/1743285512Y.0000000015>
 25. Mostaghel S, Matsushita T, Samuelsson C, Bjorkman B, Seetharaman S (2013) Influence of alumina on physical properties of an industrial zinc-copper smelting slag. Part 3—melting behaviour. *mineral processing and extractive metallurgy (transactions of the mining and metallurgy: section C)*. <https://doi.org/10.1179/1743285512Y.0000000028>
 26. Mostaghel S, Samuelsson C, Bjorkman B (2013) Influence of alumina on mineralogy and environmental properties of zinc-copper smelting slags. *Int J Miner, Metall Mater*. <https://doi.org/10.1007/s12613-013-0718-3>
 27. Wu L, Ek M, Song M, Sichen D (2011) The effect of solid particles on liquid viscosity. *Steel Res Int*. <https://doi.org/10.1002/srin.201000207>
 28. Eriksson J and Bjorkman B (2004) MgO modification of slag from stainless steelmaking. In: Proceedings of the VII International Conference on Molten Slags Fluxes and Salts, pp 455–460.
 29. Jalkina G, Teng L, Bjorkman B, Seetharaman S (2013) Effect of low oxygen partial pressure on the chromium partition in CaO-MgO-SiO₂-Cr₂O₃-Al₂O₃ synthetic slag at elevated temperatures. *Steel Res Int*. <https://doi.org/10.1002/srin.201200214>
 30. Ylipekkala J (2005) Quality management of chromium containing steel slags from melt phase to cooling. (Master's Thesis). Lulea University of Technology, Lulea, Sweden.
 31. Levin EM, Robbins CR, McMurdie HF (1964) Phase diagrams for ceramists. The American Ceramic Society, Columbus

Publisher's Note Springer Nature remains neutral with regard to jurisdictional claims in published maps and institutional affiliations.